

## ELECTRONIC SUPPLEMENTARY INFORMATION

### Synthesis of Electrospun PAN nanofibers

Table S1 shows the different electrospinning conditions for the different used PAN concentrations. The different conditions depend on the different parameters such as the PAN concentration, the solution viscosity and conductivity.

**Table S1.** Experimental conditions for the different electrospun PAN nanofibers.

Polymer	Electrospinning solution	Viscosity (cP)	Conductivity ( $\mu\text{S}/\text{cm}$ )	Experimental conditions
PAN	15.0 wt% in DMF	5936	127.1	Voltage: 18.0 kV, Distance: 150 mm, Flux: 1.5 mL/h, Needle: GA 22*.
PAN	10.0 wt% in DMF	848	110.9	Voltage: 25.0 kV, Distance: 150 mm, Flux: 1.8 mL/h, Needle: GA 23**.
PAN	8.5 wt% in DMF	381	96.6	Voltage: 27.5 kV, Distance: 200 mm, Flux: 1.8 mL/h, Needle: GA 23**.
PAN	7.0 wt% in DMF	196	86.2	Voltage: 27.5 kV, Distance: 150 mm, Flux: 1.5 mL/h, Needle: GA 23**.

\* GA 22: 12,7mm tips with 0.33mm inner diameter.

\*\* GA 23: 12,7mm tips with 0.41mm inner diameter.

It is known that the morphology of electrospun fibers depends on various operation parameters and solution properties. In fact, at higher precursor concentration the polymer chains are more tangled, which leads to the production of broader fibers. When the electrical conductivity of the solution was higher, a lower electrical field (voltage/distance) is needed for the formation of nanofibers. Finally, if precursor solution presents high viscosity, it could be electrospun by the application of a low electrical field.

In our study, the optimization of the electrospinning process has been focused on the achievement of a homogeneous and stable process followed by high productivity. In this sense, while voltage and distance were adjusted in order to present an optimal electric field, flux and needle diameter were optimized to achieve the maximum productivity (flow rate) for the fabrication PAN of nanofibers.

### Adsorption experiments over SPION loaded HPAN nanofibers in continuous mode

#### a) Experimental set-up

Adsorption experiments in continuous mode were performed using the setup depicted in Fig. S1.

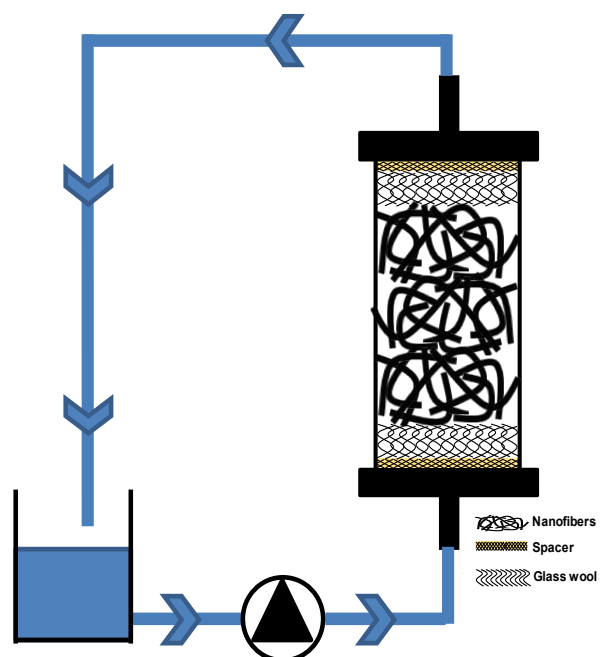


Fig. S1 Experimental set-up of As(V) adsorption in continuous mode by counterflow

*b) Physical-Chemical characterization of the lixiviation water*

Table S2. Physical-Chemical characterization of the lixiviation water

Analytical Parameter	Units	Value	Technique or analytical Method
pH	-	7.41	pHmeter
Electrical Conductivity	$\mu\text{S}/\text{cm}$	2900	Conductimetry
Turbidity	NTU	165	UNE-EN ISO 7027:2001
SST	mg/L	10	UN-EN 872:2005
DQO	mg O <sub>2</sub> /L	1.176	UNE 77004:2002
DBO <sub>5</sub>	mg O <sub>2</sub> /L	756	SM 5210 B (APHA 1992a)
DBO <sub>5</sub> /DQO	-	0.64	-
TOC	mg/L C	394.5	UNE-EN 1484:1998
TN	mg/L N	0.7	
Ammonium	mg/L NH <sub>4</sub> <sup>+</sup>	< 5	Kjeldahl method
Nitrite	mg/L NO <sub>2</sub> <sup>-</sup>	< LD	Ion Chromatography (CI)
Nitrate	mg/L NO <sub>3</sub> <sup>-</sup>	< LD	CI
Sulphate	mg/L SO <sub>4</sub> <sup>2-</sup>	< LD	CI
Chloride	mg/L Cl <sup>-</sup>	654.17	CI
Fluoride	mg/L F <sup>-</sup>	95.64	CI
Lindane	mg/L	2.52	GC-MS with hexane Liquid-Liquid extraction
Phosphate	mg/l PO <sub>4</sub> <sup>3-</sup>	< LD	Colorimetric method with ammonium molibdate and ascorbic acid
Total Phosphorus	mg/L P	5.4	ICP-MS
Total Iron	mg/L Fe	0.04	ICP-MS
Na	mg/L	38	ICP-MS
Mg	mg/L	56	ICP-MS
Al	mg/L	< 0.1	ICP-MS

K	mg/L	8	ICP-MS
Ca	mg/L	551	ICP-MS
Mn	mg/L	0.1	ICP-MS
Cu	mg/L	< 0.01	ICP-MS
Ba	mg/L	0.308	ICP-MS
Li	µg/L	< 0.1	ICP-MS
Be	µg/L	< 0.1	ICP-MS
V	µg/L	< 0.01	ICP-MS
Cr	µg/L	< 0.01	ICP-MS
Co	µg/L	< 0.01	ICP-MS
Ni	µg/L	< 0.01	ICP-MS
Zn	µg/L	< 0.1	ICP-MS
Ga	µg/L	< 0.01	ICP-MS
As	µg/L	< 0.01	ICP-MS
Rb	µg/L	< 0.01	ICP-MS
Sr	µg/L	9	ICP-MS
Mo	µg/L	< 0.1	ICP-MS
Pd	µg/L	< 0.01	ICP-MS
Ag	µg/L	< 0.01	ICP-MS
Cd	µg/L	< 0.01	ICP-MS
In	µg/L	< 0.01	ICP-MS
Cs	µg/L	< 0.01	ICP-MS
Hg	µg/L	< 0.01	ICP-MS
Tl	µg/L	< 0.01	ICP-MS
Pb	µg/L	< 0.01	ICP-MS
Bi	µg/L	< 0.01	ICP-MS

### Distribution diagrams of the nanofiber diameter for the different developed nanofibers

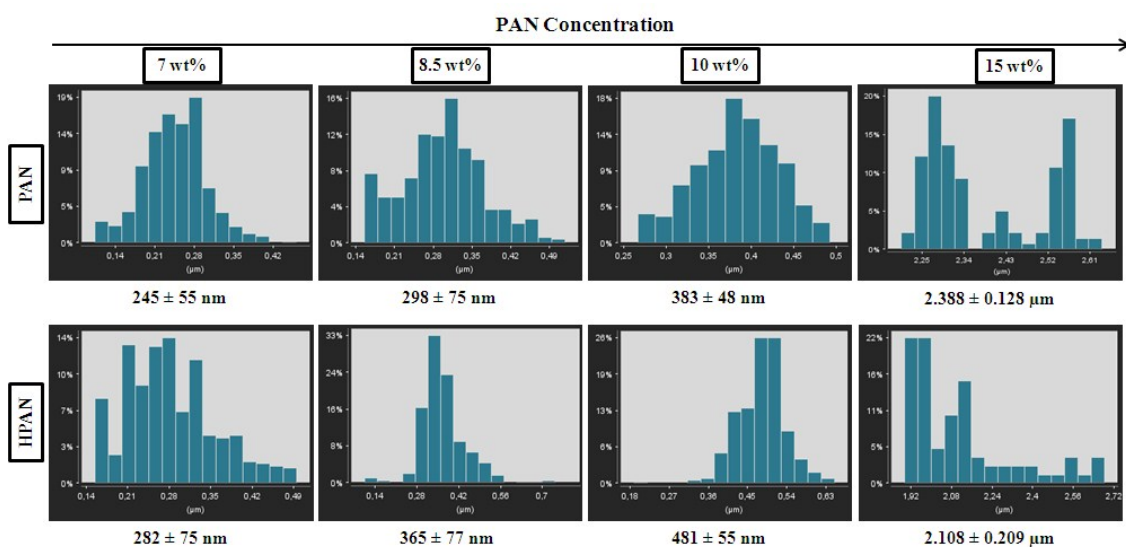


Fig. S2 Nanofibers size diameter distribution diagrams.

### Characterization of PAN and HPAN nanofibers: Fourier Transformed Infrared

ATR-FTIR spectra of electrospun PAN and HPAN nanofibers are shown in Fig. S3. For the electrospun PAN nanofibers, the peak at about  $2918\text{ cm}^{-1}$  is assigned to the stretching vibration of methylene ( $-\text{C}-\text{H}_2$ ) group. The band at  $2242\text{ cm}^{-1}$  is in correspondence with the nitrile ( $-\text{C}\equiv\text{N}$ ) stretching mode. The peak at  $1664\text{ cm}^{-1}$  corresponds with the C-C stretching mode and  $1452\text{ cm}^{-1}$  is due to the bending vibration of methylene group. In view of the principal absorption peak, electrospun PAN nanofibers present their characteristic peaks and these nanofibers can be used in the next steps of this study

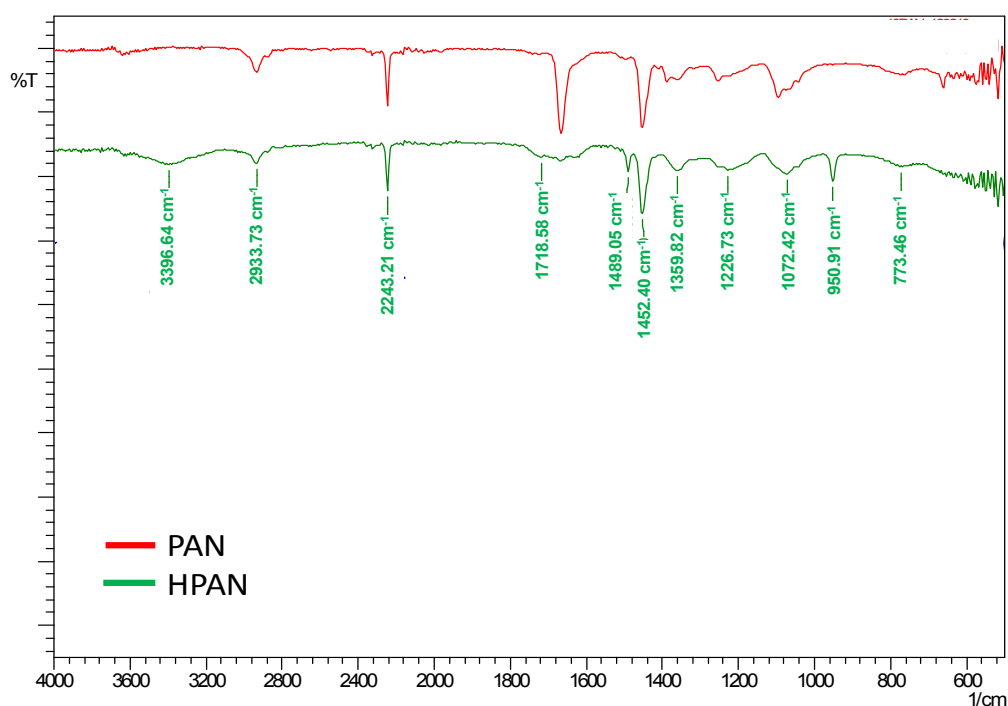


Fig. S3 ATR-FTIR spectra of PAN and HPAN nanofibers

For the HPAN nanofibers, the peak present at  $3396.64\text{ cm}^{-1}$  can be due to the stretching mode of the free-hydroxyl groups. The band at  $2243.41\text{ cm}^{-1}$  is in correspondence with the nitrile stretching mode due to the remaining nitrile groups ( $\text{C}\equiv\text{N}$ ) after the synthesis. The FT-IR spectrum shows the carbonyl absorption bands with two peaks at  $1718\text{ cm}^{-1}$  and  $1226.73\text{ cm}^{-1}$  that correspond to the stretching mode of  $\text{C}=\text{O}$  and  $\text{C}-\text{O}$ , respectively. In addition, two peaks corresponding the bending mode of the hydroxyl ( $-\text{O}-\text{H}$ ) were observed at  $1489.05$  and  $950.91\text{ cm}^{-1}$ .

### SPION loaded HPAN nanofibers synthesis

Fig. S4 shows the difference between a PAN and HPAN nanofibers after having been in contact with SPION suspension. For PAN nanofibers, there is poor fixation of SPION after 12 hours of contact with the suspension due to the low interaction between nanoparticles and the functional groups of PAN fibers. As result, homogeneously dark suspension is visible in Fig.4 left as all SPION tend to stay in the suspension instead of attaching on the surface of the fibers. On the contrary, for HPAN nanofibers (Fig.4 right) practically all SPION are attached onto the nanofibers, as indicated by the black mass floating on top of the vessel, while the suspension is almost transparent. This fact reveals that the presence of carboxylic groups on the HPAN nanofiber surface provide a corresponding ligand exchange mechanism with SPION and it produce a strong interaction that fix the SPION on HPAN nanofibers.

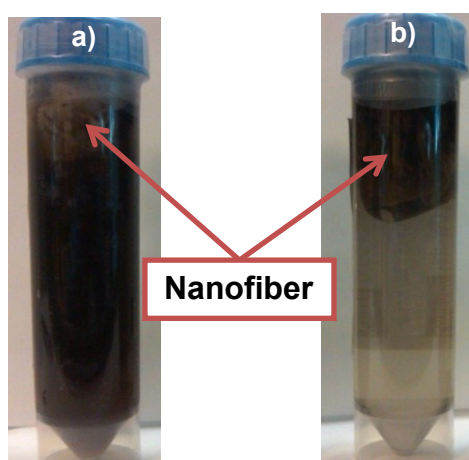


Fig. S4 Electrospun PAN (a) and HPAN (b) nanofibers in contact with SPION suspension after 12 hours

### Adsorption experiments over HPAN nanofibers in batch mode

Table S3. Adsorption capacity of different PAN and hydrolized-PAN nanofibers without SPION load.

Sample	Maximum Adsorption Capacity (mmol As(V)/g SPION)
PAN-10	0.09
PAN-15	0.03
HPAN-7	0.04
HPAN-8.5	0.01
HPAN-10	0.11
HPAN-15	0.01

### Swelling effect of HPAN-10-SPION nanofibers



Fig. S5 HPAN-10-SPION nanofibers after the SPION impregnation (a) and 2 hours later in a water solution (b)